Smart Structures and Systems, *Vol. 34, No. 5 (2024) 299-310*
https://doi.org/10.12989/sss.2024.34.5.299

Experimental study on impedance-based damage detection considering temperature effect and operating condition

Jong-Won Lee*

Department of Architectural Engineering, Namseoul University,
91 Daehak-ro, Seobuk-gu, Cheonan-si, Chungcheongnam-do 31020, Republic of Korea

(*Received March 7, 2023, Revised December 5, 2024, Accepted December 6, 2024*)

Abstract. Impedance-based damage detection technique has been pointed out as a useful method for structural health monitoring. However, it is needed to consider the temperature effect on the impedance signature to apply this technique in real structures. Also, for practical application, it is advantageous to consider the operating conditions such as vibration and live load. And, the correlation between the measured impedance data and the analysis results can improve the capability of structural health monitoring. In this study, an impedance-based damage detection method considering the temperature effect and operating conditions is experimentally researched for an aluminum beam, and the correlation between the impedance damage indices obtained from experiment and the equivalent bending stiffness for the cracked beam calculated by analysis is investigated. The long-term measurement under vibration is carried out, and it is found that the damage can be clearly estimated, while monitoring the warning criterion together, after compensating the temperature effect. It is also found that as the crack size increases, the variation in the damage indices increases, and the correlation between the impedance damage index due to crack propagation and the analyzed equivalent bending stiffness of the cracked beam is partially identified.

Keywords: damage detection; impedance; operating condition; practical application; temperature effect

1. Introduction

The electromechanical impedance-based damage detection technique is a useful one for structural health monitoring of various types of structures, and related researches have been widely carried out. However, due to the environmental effect such as temperature change on the impedance signature measured by the piezoelectric sensor, it is difficult to effectively apply this method in real structures. Therefore, in order to efficiently apply the impedance-based damage detection technique to real structures, it is necessary to consider the temperature effect, which is a representative environmental noise. Also, for practical structural health monitoring, it is advantageous to measure data during operation of structure and analyze data considering the operating conditions such as vibration and live load. In addition, it is supposed that more efficient structural health monitoring can be performed if the correlation between the measured data and the analysis results of the corresponding structure is identified.

Abbas *et al*. (2021) have identified the presence of fatigue crack in stainless steel beam using electro-mechanical impedance approach and estimate the effect of temperature variation on the impedance. The effective frequency shift technique was modified for the compensation of temperature effect over the impedance signature of the PZT (lead zirconate titanate) sensor. Rabelo *et al*. (2017) have proposed a technique on the damage detection of incipient faults in rotating shafts by using a real-time impedance-based method. A temperature compensation technique was proposed based on a hybrid optimization method associated with different damage metrics. Du *et al*. (2023) have studied the bolt loosening monitoring method using the deep convolutional neural network for the electromechanical impedance. The network consists of a temperature compensation subnetwork, trained using the experimental results under various temperature conditions, and a damage identification subnetwork. Zhang *et al*. (2019) have studied an electromechanical impedance-based technique to detect ice accretion on the stay cables of cable-stayed bridge. The changes in structural stiffness and mass due to the ice covered were considered as primary characteristics, whereas the change in temperature was corresponded to the disturbing factor. Gianesini *et al*. (2021) have proposed a new methodology to compensate for the temperature effect in the electromechanical impedance technique. The temperature and frequency dependences of the impedance signatures were observed experimentally on the aluminum beams and steel pipe, and a simple analytical polynomial-based temperature compensation method was applied. Hong *et al*. (2012) have experimentally examined the temperature-compensated damage monitoring in steel girder connections by using the wireless acceleration-impedance sensor nodes. A temperature-compensated damage monitoring scheme was designed by using the temperature compensation model based on regression analysis. Baral *et al*. (2023) have studied on temperature compensation in the impedance by

*Corresponding author, Ph.D., Professor,
E-mail: jwlee.kimm@gmail.com

http://www.techno-press.org/?journal=sss&subpage=7
ISSN: 1738-1584 (Print), 1738-1991 (Online)

compensating values calculated based on experiments on piezo sensors both in a free boundary condition and in a bonded condition on a metallic host structure. The variation in the first natural frequency values for the unbonded piezo sensor at different temperatures was used to develop the compensation algorithms. Antunes *et al*. (2019) have developed a method applied to damage detection in pipelines, including a technique for compensating the temperature effect in electromechanical impedance-based structural health monitoring. The experiments were conducted while changing the temperature, and compensation algorithms for frequency shift and amplitude change were proposed, respectively. Silva *et al*. (2021) have proposed a new method to compensate temperature effect based on a transfer component analysis, a subtype of transfer learning, of the features from a source domain to another target domain. They assumed only the labeled features data in the healthy condition and damaged state in a specific temperature as source data. Campos *et al*. (2019) have presented a new feature extraction approach insensitive to temperature variations for effective electromechanical impedance-based structure health monitoring for real structures. This method was based on the statistical criterion algorithm, which extracts the number of significant resonance peaks from the electrical impedance signatures. De Castro *et al*. (2019) have proposed a new index in the electromechanical impedance-based damage detection technique for structure feature extraction based on the cross correlation signal processing technique that can be applied in real noisy environment. The proposed index was evaluated in the frequency domain and time domain, and experiments were carried out on a damaged aluminum structure subject to various signal noise levels. Huynh *et al*. (2018) have proposed a principal component analysis-based algorithm to filter out temperature effects on electromechanical impedance monitoring of prestressed tendon anchorages. The algorithm was experimentally evaluated by distinguishing temperature changes from prestress-loss events in a prestressed concrete girder.

In the previous studies, the impedance-based damage detection methods considering the temperature effect in various ways have been mainly studied for practical application. However, for more practical application, it is advantageous to acquire data during operation, so it is supposed that additional consideration for operating conditions is needed. And, the previous studies mainly detect the damage by experimentally identifying the relationship between the damage and the impedance damage index. Due to the complexity of PZT patch-adhesive-host structure coupled structural system and the difficulty of dynamic analysis in the high-frequency range, there may be difficulties to correlate changes in the impedance signatures to physical parameters of structures and could not provide further information about the nature of damage (Yan and Chen 2010). However, it is considered necessary to assess the current state of the structure more accurately and predict the structural behavior using the analysis model by identifying the correlation between the impedance signature and the analysis model for structural damage.

In this study, for the practical application of the impedance-based damage detection technique, an experimental study considering not only the temperature effect but also the operating conditions such as vibration and live load is carried out, and additionally, the experimental results are compared with the analytical values. That is, an impedance-based damage detection method using the impedance signatures measured under vibration considering temperature effect is experimentally researched for an aluminum beam, and the experiment is also performed while changing the applied stress. Moreover, the correlation between the impedance damage indices obtained from experiment and the equivalent bending stiffness for the cracked beam calculated by analysis is partially identified.

2. Damage index of impedance

Liang *et al*. (1996) have studied the relationship between the electromechanical impedance measured from the piezoelectric sensor attached to the structure and the mechanical impedances of the structure and piezoelectric sensor. That is, if damage occurs in the structure near the attached piezoelectric sensor, the structural characteristics change, and the impedance signature measured from the piezoelectric sensor changes. Therefore, the damage of the structure can be estimated by comparing and analyzing the impedance signature before and after the damage. However, the impedance signature can be changed not only due to the damage but also the other factors such as temperature change and durability of the piezoelectric sensor (Na and Baek 2018).

The damage index quantifying the impedance change before and after the damage can be used for comparative analysis. In impedance-based damage estimation techniques, the most widely used are the root mean square deviation based damage index in Eq. (1), which is more sensitive to variations in amplitude of the impedance, and the correlation coefficient deviation based damage index in Eq. (2), more sensitive to changes in the shape between the impedance signatures, such as frequency shifts (Baptista *et al*. 2011).

$$DI1 = \sqrt{\frac{\sum_{i=1}^{n}\{Re(Z_i^d) - Re(Z_i^0)\}^2}{\sum_{i=1}^{n} Re(Z_i^0)^2}} \tag{1}$$

$$DI2 = \frac{1}{N}\frac{\sum_{i=1}^{n}\{Re(Z_i^0) - \overline{Z^0}\}\{Re(Z_i^d) - \overline{Z^d}\}}{\sigma_{Z^0}\sigma_{Z^d}} \tag{2}$$

where Z is the measured impedance, $Re(Z)$ denotes the real impedance, i is the frequency, 0 denotes the healthy or reference state, d denotes the damaged or comparison state, $\overline{Z^0}$ and $\overline{Z^d}$ are the means of the real impedances and σ_{Z^0} and σ_{Z^d} are standard deviations of the real impedances.

If the values of the $DI1$ and $DI2$ are 0 and 1, respectively, it can be assumed that the 2 impedance signatures being compared are the same. As the difference between the 2 impedance signatures increases, the $DI1$

will increase from zero and the $DI2$ will decrease from one. The damage indices in Eqs. (1) and (2) will be calculated by including the effect of temperature variation and possible environmental noise in addition to the impedance change due to structural damage. Therefore, in order to detect the damage of the structure using the impedance damage index, the other factors such as temperature change in addition to the effect of the damage should be considered.

3. Experimental method

For the study of the impedance-based damage detection method considering the temperature variation and operating conditions of the structure such as vibration and applied stress, a cantilever aluminum beam with a length of 1 m and a solid rectangular cross section (width 40 mm, height 60 mm) was built as shown in Fig. 1. The 20 t plate at the left end of the specimen shown in Fig. 1 was fastened to a strong column using high tensile bolts, and the column was attached to the laboratory floor so that a certain fixed end effect was realized. On the other hand, the experiment was carried out by adding a tip mass to the free end as shown in Fig. 1.

For the impedance measurement, the PZT sensors of 10(L) × 10(W) × 0.3(T) size were used. PZT 1 and 2 were attached at locations 150 and 50 mm away from the fixed end, respectively as shown in Fig. 2. To observe the change of the impedance signature due to the temperature variation only of PZT sensor, PZT 3 was located near PZT 1 and 2, and measurement was performed together without attaching it to the specimen. In addition, to estimate the vibration quantity of the specimen during the impedance measurement under vibration, accelerometers (Acc 1-Acc 4) were installed at the locations shown in Fig. 2. Here, although the 20t plate was fixed as mentioned above, an accelerometer (Acc 1) was installed on the 20t plate because it was supposed that the full fixed effect would not be realized. On the other hand, the damage test was carried out by increasing the crack size at a location 100 mm away from the fixed end as shown in Fig. 2. The air temperature near the specimen was measured.

In the impedance tests, an impedance analyzer (Keysight; E4990A) was used. The preliminary tests were carried out for each PZT sensor to choose the target sweep frequency bands for estimating the damage properly. In the electromechanical impedance technique for structural health monitoring, the PZT sensor is subjected to an alternating voltage excitation from an impedance analyzer, sweeping through a particular frequency range, generally 30–400 kHz (Bhalla *et al*. 2009). Therefore, the sinusoidal voltage was applied to each PZT sensor while sweeping over the frequency range of 30 kHz to 400 kHz using the impedance analyzer, and the impedances for this were also measured in each PZT sensor for the healthy state. The target frequency range should include the resonance peak to facilitate the detection of small structural changes (Tawie and Lee 2010). The target sweep frequency bands for the PZT sensors were set to 230-250 kHz for PZT 1, 200-220 kHz for PZT 2, and 195-205 kHz for PZT 3, respectively because each peak exists in the real impedance plot in those frequency ranges. That is, in the impedance tests, a sinusoidal voltage with an RMS (root mean square) value of 50 mV was applied to each PZT sensor while sweeping frequencies in each frequency band, and the impedance was measured for 5 seconds.

Fig. 1 Experimental setup

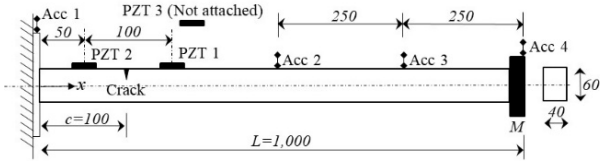

Fig. 2 Sensor locations (lengths in mm)

For the impedance measurement under vibration, the free vibration was generated using the impact hammer method. To estimate the vibration quantity, the accelerations were measured from 4 accelerometers shown in Fig. 2 with the sampling rate of 10 kHz for 5 seconds using a data acquisition device (NI cDAQ-9178, NI 9234) and software (LabView).

The experiments were carried out in 3 stages. In the 1st stage (Chapter 4), the experiment was conducted to estimate the effect of applied stress and vibration on the impedance signature for the healthy state. That is, in order to change the stress applied on the PZT sensor attachment location, the impedance was measured while changing the tip mass of the specimen. In addition, in order to estimate the effect of vibration on the impedance signature, the impedances in the non-vibration state of the specimen and during vibration were measured under the same conditions. In the 2nd stage (Chapter 5), the long-term measurement was performed on the specimen for the healthy state in order to evaluate the effect of temperature variation on the impedance signature. After fixing the tip mass to 2.83 kg, the impedance was measured 3-4 times a week for a total of 60 times from May 18, 2022. In the 3rd stage (Chapter 6), in order to estimate the effect of damage on the impedance signature, the impedance was measured while increasing the crack size step by step at the crack location shown in Fig. 2. The cracks were inflicted by making fine saw cuts of the specimen, and 6 cases of damages were introduced by changing the depth of the inflicted crack.

4. Effect of applied stress and vibration

In order to estimate the effect of the applied stress, which is one of the operating conditions of the structure, the impedance tests were conducted while changing the applied stress at the PZT attachment location. The impedances were measured under different applied stress conditions in 11 cases (Case 0-10), that is, while adding 0.565 kg step by

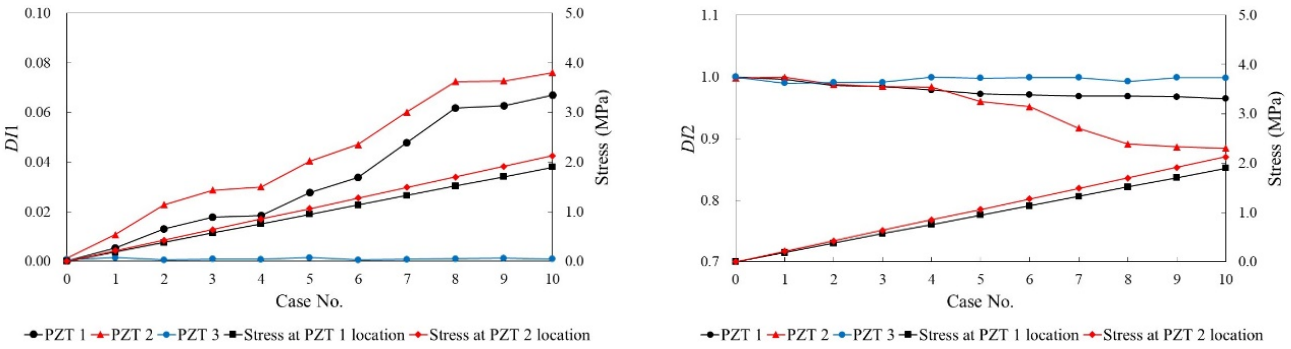

(a) $DI1$ (b) $DI2$

Fig. 3 Relation between applied stress and damage index

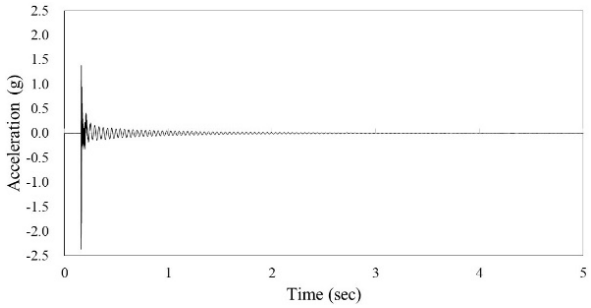

Fig. 4 Acceleration time history

step from 0 kg to 5.65 kg to the tip mass in Fig. 2.

The $DI1$ in Eq. (1) and the $DI2$ in Eq. (2) for the 11 cases are compared in Fig. 3 and this is the result of temperature compensation described later. When the tip mass was 0 (Case 0), the tests were performed 2 times, and in Fig. 3, the value for 0 on the x-axis represents the index between the 2 tests with the tip mass of 0. The rest of the results are the indices calculated with reference to the impedance of Case 0. It can be found that as the degree of applied stress increases, the $DI1$ increases gradually more than zero and the $DI2$ decreases gradually less than one. The impedance of PZT 2 is more affected by the applied stress than that of PZT 1, which is considered to be because the applied stress is larger at the attachment location of PZT 2. In addition, it can be seen that the index of the impedance of PZT3, not attached to the specimen, is almost constant even when the applied stress changes. This result indicates that the impedance is affected by applied stress, and it is supposed that the effect of live load on impedance should be considered for the future practical application of the impedance-based damage detection method. However, in the long-term measurement and damage test following this study, the experiments were performed with the tip mass

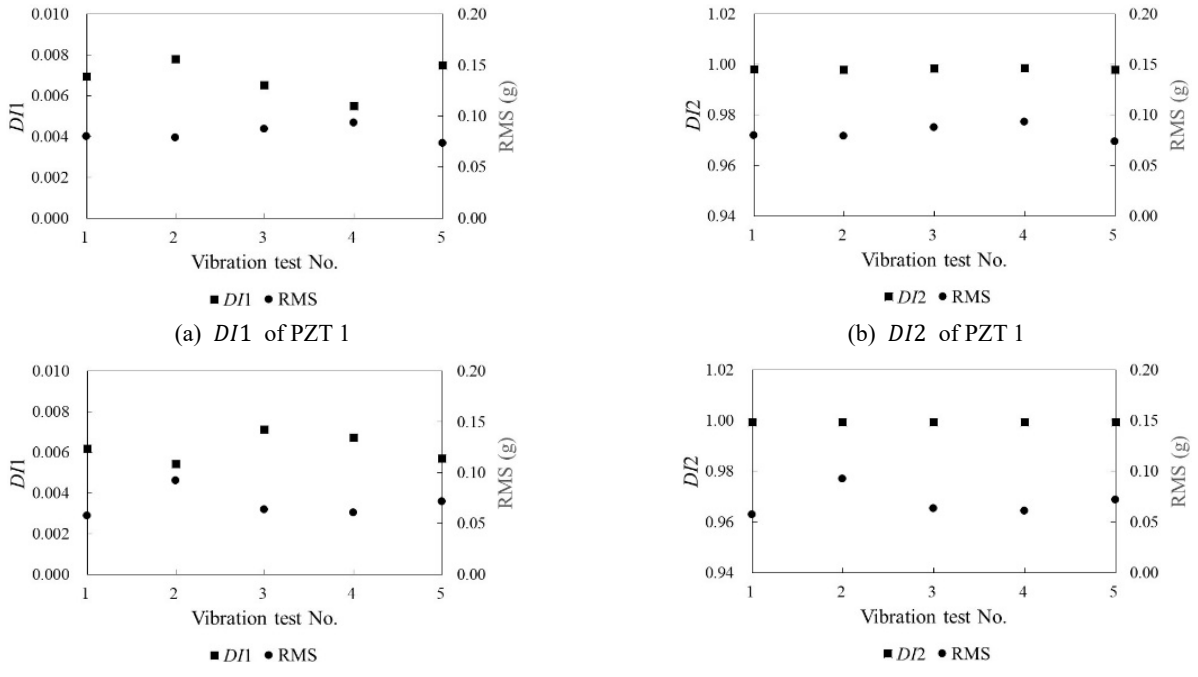

(a) $DI1$ of PZT 1 (b) $DI2$ of PZT 1

(c) $DI1$ of PZT 2 (d) $DI2$ of PZT 2

Fig. 5 Relation between RMS of acceleration and damage index

Table 1 $DI1$ and $DI2$ for each case

Case No.	Tip mass (kg)	PZT 1		PZT 2	
		$DI1$ (%)	$DI2$	$DI1$ (%)	$DI2$
0	0	0.562	0.998	0.455	0.999
1	0.565	0.328	0.999	0.419	0.999
2	1.130	0.422	0.999	0.364	0.999
3	1.695	0.579	0.999	0.410	0.999
4	2.260	0.846	0.997	0.650	0.999
5	2.825	0.684	0.998	0.623	0.999
6	3.390	0.660	0.995	0.516	0.999
7	3.955	0.726	0.998	0.563	0.999
8	4.520	0.532	0.999	0.474	0.999
9	5.085	0.492	0.999	0.522	0.999
10	5.650	0.302	0.999	0.404	0.999

fixed.

On the other hand, the impedance tests were carried out to estimate the effect of vibration on the impedance by measuring the impedance under vibration of the host structure. In the impedance test for the 11 cases mentioned above, the impedance measurements under free vibration, induced by the impact hammer method, were performed 5 times for each case, and the impact strength was adjusted so that the vibration quantity was different for each of the 5 times. A time history of the acceleration measured in Case 5 (tip mass is 2.825 kg) by the accelerometer installed at the free end (Acc 4 in Fig. 2) is shown in Fig. 4. The impedances were also measured in the non-vibration state.

The $DI1$ and $DI2$ of the impedance measured during the 5 vibration tests were calculated with reference to the impedance measured in the non-vibration state, and those are compared in Fig. 5 to the average of the RMS values calculated from the accelerations measured from the 4 accelerometers. Fig. 5 is an example of one of the results of 11 cases, which is the result for Case 5 (tip mass is 2.825 kg), and the long-term measurement and damage test following this study were carried out under the condition of this tip mass. For all 11 cases, the average for the 5 vibration cases of the $DI1$ and $DI2$ calculated from the impedances measured at PZT 1 and 2 are shown in Table 1. Here, the impedance tests in the non-vibration and vibration states for a specific case were performed under the same temperature and applied stress conditions.

As shown in Table 1, overall, the $DI1$ is less than 1% and the $DI2$ is more than 0.995, therefore it is considered that the change in the impedance signature due to vibration is insignificant. Also, as shown in Fig. 5, it can be found that there is almost no correlation between the vibration quantity and the indices. That is, since impedance is the signature of the high frequency in the kHz range, it is supposed that the low frequency structural vibration has little effect on the impedance. In the subsequent long-term measurement and damage test, the impedance measured under vibration is used in all analysis to proceed research.

5. Long-term measurement and damage detection considering temperature effect

The long-term measurement was performed with the tip mass fixed at 2.825 kg. The $DI1$ and $DI2$ of impedances, measured at PZT 1 and 2 under vibration and PZT 3 under non-vibration, calculated with reference to the impedances measured for the 1st test in the healthy state on May 18, 2022 (23.7°C) were obtained as shown in Fig. 6, and compared with the temperature change. The impedance

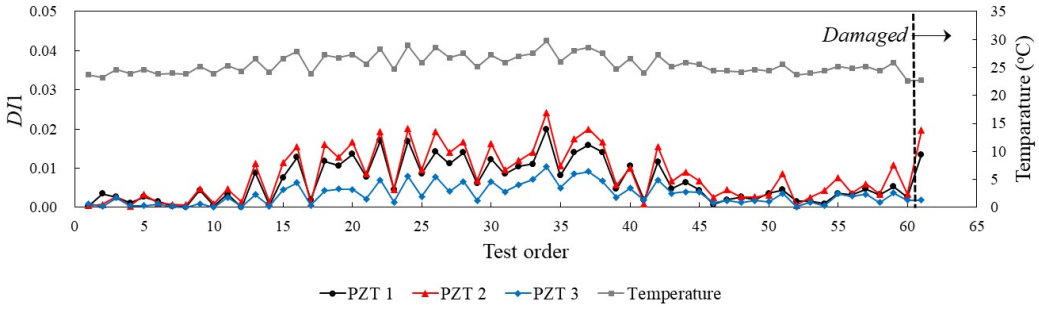

(a) $DI1$

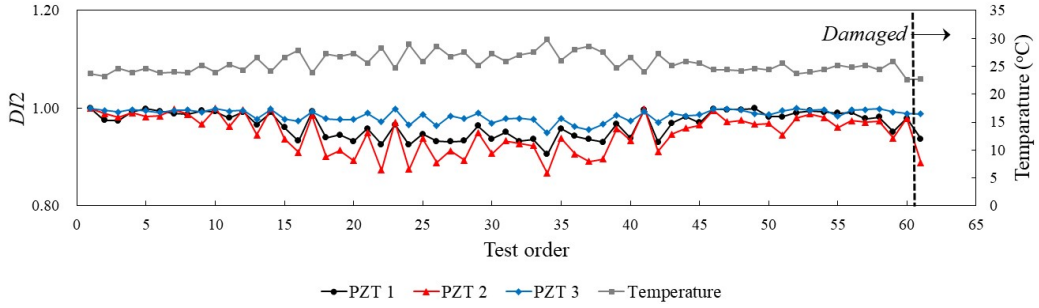

(b) $DI2$

Fig. 6 Variation of damage indices and temperature

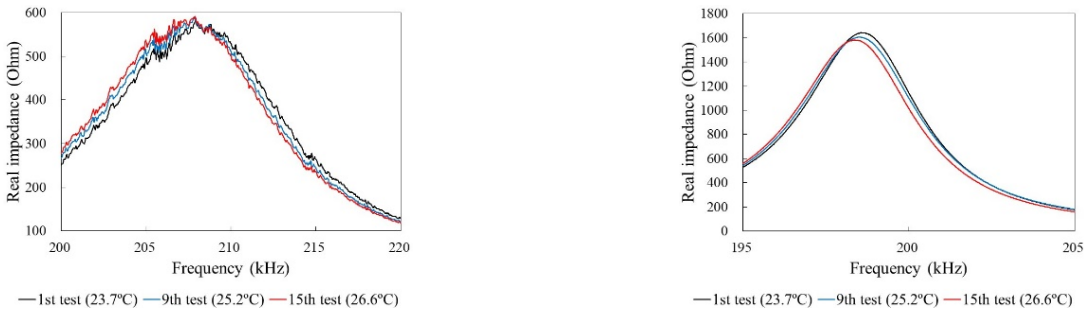

(a) PZT 2 (b) PZT 3

Fig. 7 Variation of real impedance due to temperature change

tests were carried out 3-4 times a week for a total of 60 times for the healthy state.

The $DI1$ and $DI2$ in the healthy state before the damage occurred were calculated to be greater than zero and less than one, respectively. Therefore, it is considered that the differences between the impedances are due to the temperature change. After the 60th test, a crack was generated at the location shown in Fig. 2, and the impedance test (the 61st test) was carried out. This is Damage Case 1 explained later. Since the damage indices after the damage are calculated by including the temperature and damage effects, if only the damage indices are monitored, it is difficult to estimate the damage. In the case of PZT 3, not attached to the specimen, the variations in the damage indices due to temperature change are smaller than those of PZT 1 and 2, which is considered to be because the impedance changes only under the influence of the temperature change of the sensor itself. That is, the variations in the damage indices from the impedances of PZT 1 and 2, attached to the specimen, are larger than those of PZT 3, and this is supposed to be because they include all the effects of temperature changes on sensor, structure, and adhesive.

In order to examine the variation of the impedance signature due to temperature change, the real impedances measured for the healthy state in the 1st test (23.7°C), 9th test (25.2°C) and 15th test (26.6°C) are compared in Fig. 7 for PZT 2 and 3, respectively. Here, the impedance signatures for PZT 2 were measured under vibration. It can be found that the frequency shift and amplitude change of the impedance signatures are occurred due to temperature change. It has been also studied that the temperature change causes the shift in the frequency and variation in the amplitude of the impedance signatures (Baptista *et al.* 2011). As mentioned above, the $DI1$ is more sensitive to variations in amplitude of the impedance and the $DI2$ is more sensitive to the frequency shifts between the impedances, so it is supposed that the temperature change

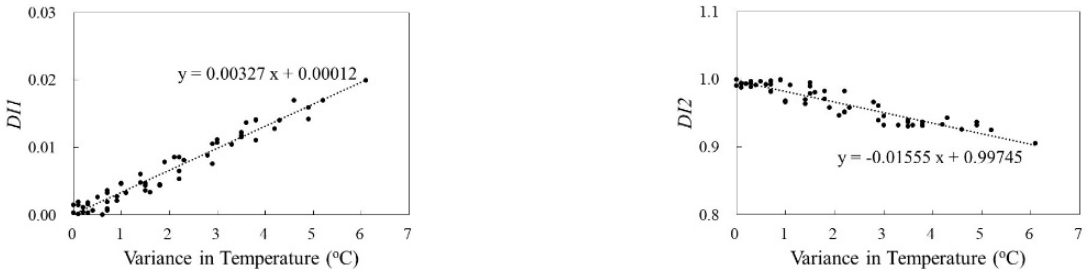

(a) $DI1$ (b) $DI2$

Fig. 8 Relationship between temperature change and damage index (PZT 1)

(a) $DI1$ (b) $DI2$

Fig. 9 Relationship between temperature change and damage index (PZT 2)

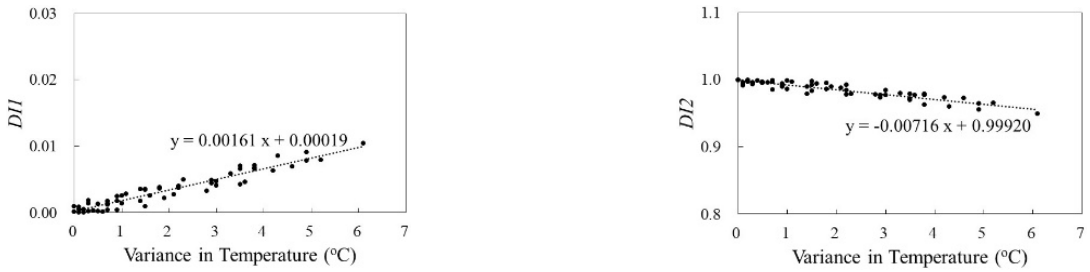

(a) $DI1$ (b) $DI2$

Fig. 10 Relationship between temperature change and damage index (PZT 3)

affects both the change of the $DI1$ and $DI2$.

For impedance-based damage estimation considering the temperature effect, the changes of the impedance damage indices according to the temperature variation are analyzed as shown in Figs. 8-10. Here, the results of PZT 1 and 2 are the damage indices obtained from the impedances measured under vibration, and the results of PZT 3 are measured under non-vibration. The temperature changes were calculated as the absolute values of the temperatures changed based on 23.7°C, which is the temperature for the 1st test in the healthy state, and the changes in the damage indices from the 1st to the 60th test performed for the healthy state were analyzed for PZT 1, 2 and 3, respectively. It can be found that the $DI1$ and $DI2$ have an approximate linear relationship with the amount of temperature change, and the $DI1$ is a proportional and the $DI2$ is an inverse proportional relationship. Therefore, after performing linear regression analysis on each data, the relationships between the temperature change amounts and the damage indices were obtained as shown in Figs. 8-10.

According to the results of the linear regression analysis, in the case of the $DI1$, for PZT 1, 2 and 3, changes of about 0.33%, 0.40%, and 0.16%, respectively, and in the case of the $DI2$, changes of about -0.016, -0.023, and -0.0072 occur when the temperature changes by 1°C. In the case of PZT 3, the sensitivities to temperature change are lower than those of PZT 1 and 2, which is considered to be because the temperature effect of the structure and adhesive was excluded because it was not attached to the specimen.

Damage detection with compensation of temperature effect was performed based on the results of the linear regression analysis. The compensation was carried out by calculating the damage indices for the corresponding temperature change using the regression analysis linear equation and subtracting those from the measured damage indices. That is, the changes of the damage indices due to the temperature change could be excluded and the changes of those caused by the damage made. The $DI1$ and $DI2$ before and after the compensation from the results of the 31st test for PZT 1, 2 and 3 are shown in Figs. 11-16. Here,

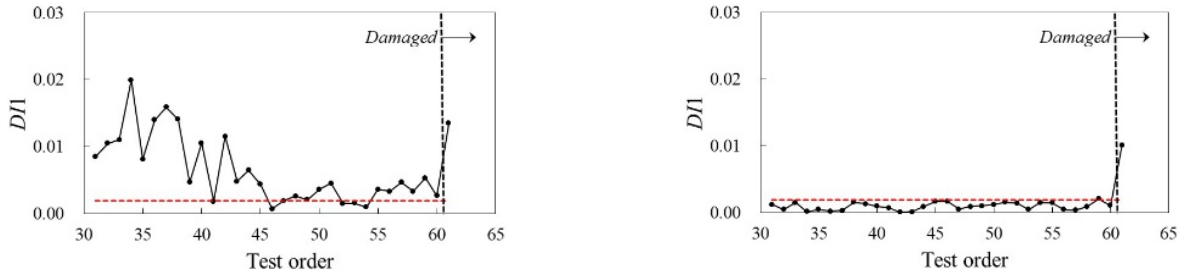

(a) Before compensation (b) After compensation

Fig. 11 Temperature compensated damage index, $DI1$ (PZT 1)

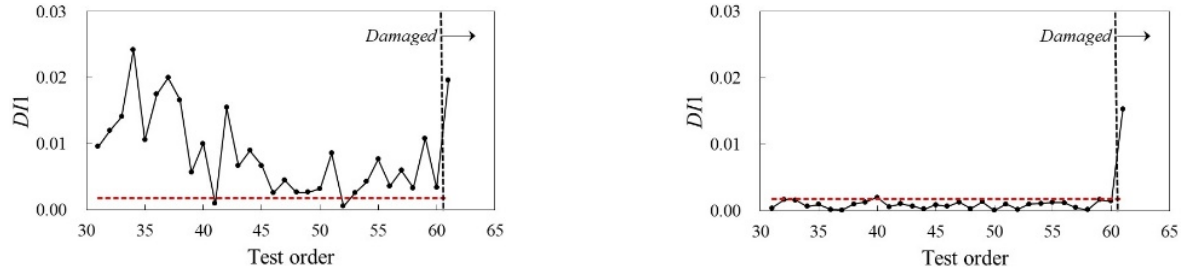

(a) Before compensation (b) After compensation

Fig. 12 Temperature compensated damage index, $DI1$ (PZT 2)

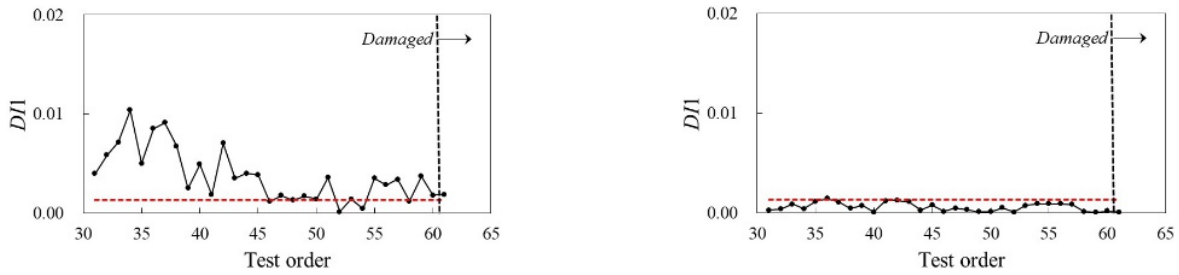

(a) Before compensation (b) After compensation

Fig. 13 Temperature compensated damage index, $DI1$ (PZT 3)

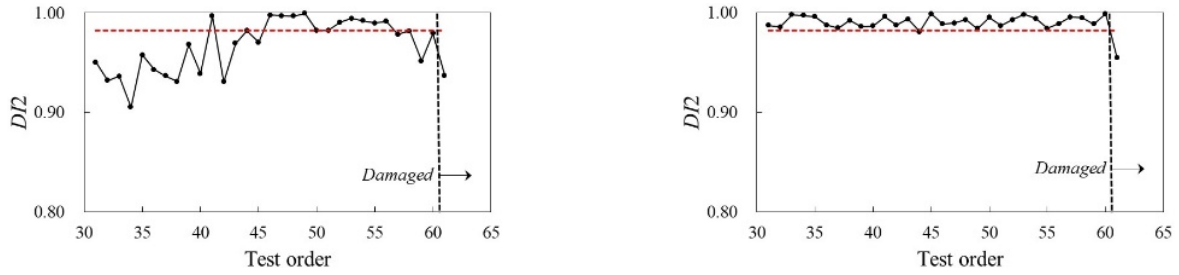

(a) Before compensation (b) After compensation

Fig. 14 Temperature compensated damage index, $DI2$ (PZT 1)

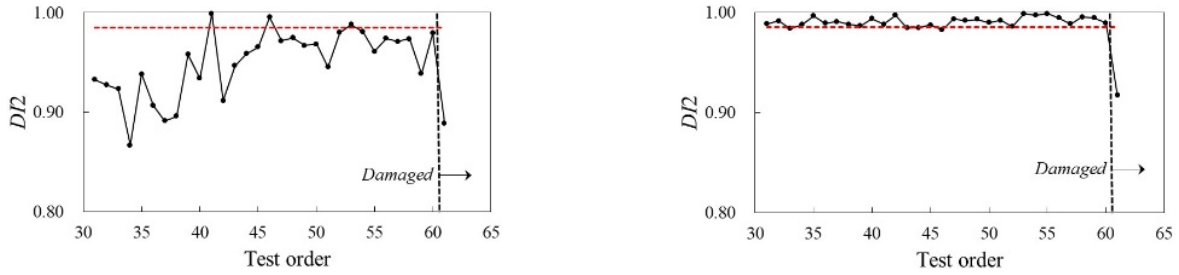

(a) Before compensation (b) After compensation

Fig. 15 Temperature compensated damage index, $DI2$ (PZT 2)

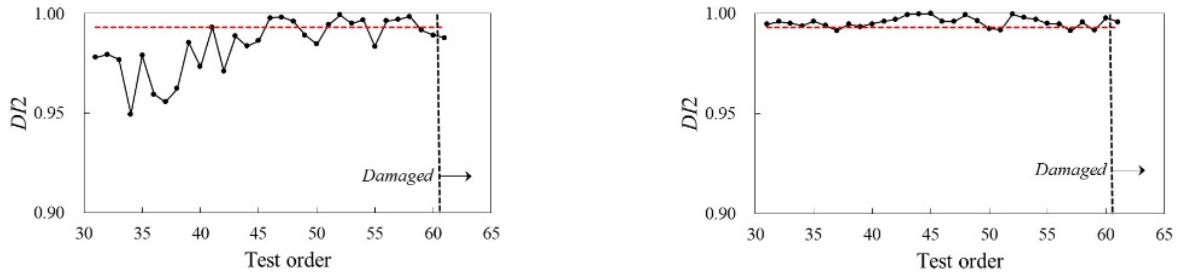

(a) Before compensation (b) After compensation

Fig. 16 Temperature compensated damage index, $DI2$ (PZT 3)

until the 60th test, it is the test in the healthy state, and the 61st test in the damaged state (Damage Case 1 explained later).

It is necessary to establish warning criteria in structural health monitoring. Assuming that the distribution of the differences between the damage indices obtained using the regression analysis linear equation and the measured damage indices is normal distribution, and applying the empirical rule, 3 times the standard deviation of the differences was set as a warning criterion, and this is indicated by a red dotted line in Figs. 11-16 together. Here, the standard deviation is the value for the test results in the healthy state.

It is supposed that the warning criterion can be improved to a more appropriate one by utilizing wider temperature range and more long-term measurement data in

the future. As shown in Figs. 11-16, it is difficult to estimate the damage before compensating the temperature effect, but after compensating the temperature effect, it can be found that the damage can be clearly estimated while monitoring the warning criterion together. That is, if the temperature effect is compensated, the damage indices in the healthy state are almost within the warning criterion, but after the damage, it can be clearly estimated because it is significantly deviated from the warning criterion. In the case of the unattached PZT 3, it can be found that the changes in the damage indices due to the damage are excluded, and those due to the temperature effect occur within the warning criterion even after the damage.

6. Damage index and equivalent bending stiffness

The impedance tests were performed while increasing the crack size (a/h), shown in Fig. 17, step by step at the crack location (c/L = 0.1) shown in Fig. 2, to experimentally study the effect of crack size on the impedance damage index. The cracks were inflicted by making fine saw cuts of the beam shown in Fig. 18. Six cases of damages were introduced, and the damage scenario is shown in Table 2.

The real impedances for PZT 2, measured under vibration, are compared for Intact Case, Damage Case 1 and 2 in Fig. 19. The impedance signature for Intact Case is the same as that of the 1st test shown in Fig. 7(a), and measured at 23.7°C. The temperatures corresponding to Damage Case 1 and 2 were 22.5°C and 22.7°C, respectively. It can be found that the frequency shift and amplitude change of the impedance signatures are occurred due to damage and temperature change.

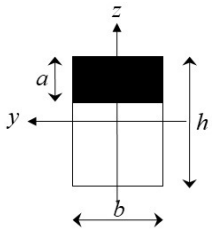

Fig. 17 Configuration of cracked section

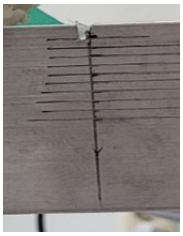

Fig. 18 Inflicted crack (a/h = 0.085)

Table 2 Damage scenario

Damage case	Crack size, a/h	Crack location, c/L
1	0.085	0.1
2	0.117	
3	0.167	
4	0.225	
5	0.308	
6	0.392	

The $DI1$ and $DI2$ measured from PZT 1 and 2 for each healthy and damaged case are shown in Fig. 20, where the damage indices were obtained from the impedances measured under vibration and temperature compensated. It can be found that as the crack size increases, the $DI1$ increases gradually more than zero and the $DI2$ decreases gradually less than one. In Fig. 20, the values for 0 on the x-axis represent the damage indices between the 2 healthy states.

When a crack occurs in a beam of solid rectangular section, the equivalent bending stiffness of the cracked beam in Eq. (3) was derived using the energy balance approach (Yang *et al*. 2001).

$$EI_c = \frac{EI}{1 + \frac{EIR(a,c)}{\left\{1+\left(\frac{x-c}{k(a)a}\right)^2\right\}}} \tag{3}$$

where c is the distance to crack location from the fixed end, a is the crack size as shown in Fig. 17, I and I_c are the area moments of inertia of the uncracked and cracked section, respectively and E is the Young's modulus. Hence, the equivalent bending stiffness of the cracked beam can be defined by the distance along the beam x, the crack location c and the crack size a using Eq. (3). Details of $R(a,c)$ and $k(a)$ are explained in the preceding study (Yang *et al*. 2001).

Fig. 21 shows the variation of the normalized equivalent bending stiffness along the beam length calculated from Eq. (3) when the crack location (c/L) is 0.1 for the beam shown in Fig. 2. It can be found that the stiffness reduction is highly concentrated near the crack location, and reach zero at a location far away from the crack. It can be also found that the stiffness reduction near the crack location becomes lager as the crack size increases.

In order to investigate the correlation between the impedance damage index due to crack propagation and the equivalent bending stiffness of the cracked beam, the

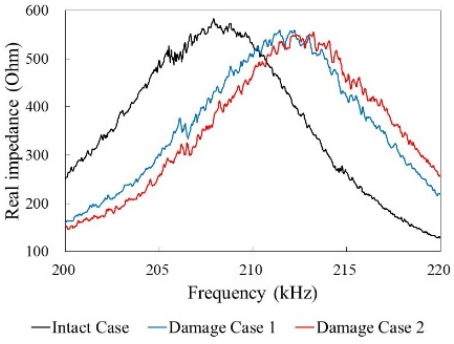

Fig. 19 Variation of real impedance due to damage and temperature change

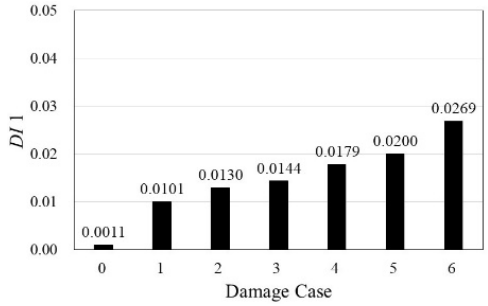

(a) $DI1$ of PZT 1

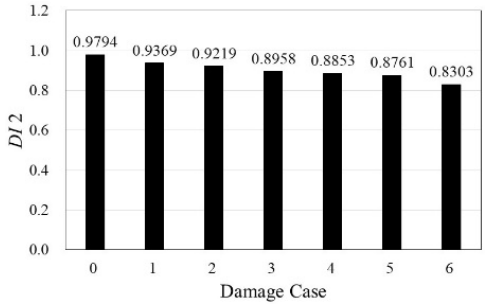

(b) $DI2$ of PZT 1

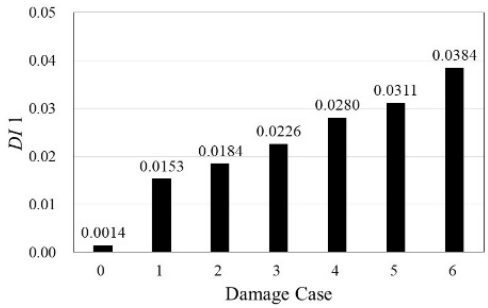

(c) $DI1$ of PZT 2

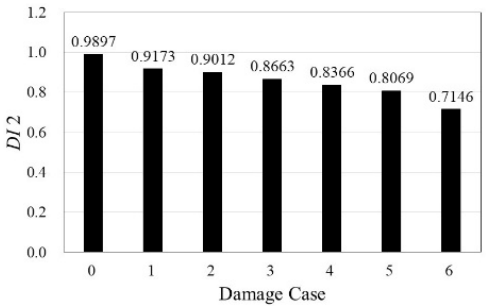

(d) $DI2$ of PZT 2

Fig. 20 Damage index for each damage case

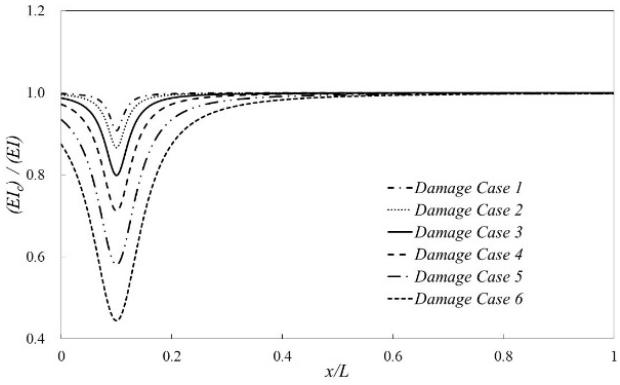

Fig. 21 Variation of equivalent bending stiffness

change in the damage index according to the crack size and the equivalent bending stiffness at a crack location (c/L = 0.1) are compared in Fig. 22. That is, the $DI1$ and $DI2$ measured from PZT 1 and 2 are compared with the equivalent bending stiffness of the cracked section. For convenience, the equivalent bending stiffness was compared with $(EI)/(EI_c)$ and the $DI2$ with $1 - DI2$.

In Fig. 22, it can be found that the variance in the damage indices increase as the equivalent bending stiffness at the crack location decreases due to crack propagation. Correlation coefficients between the damage index and analyzed equivalent bending stiffness at the corresponding crack location for 6 damage cases were calculated. The correlation coefficients between $DI1$ (PZT 1 and 2) and $(EI)/(EI_c)$ are 0.979 and 0.956, respectively, and those between $1 - DI2$ (PZT 1 and 2) and $(EI)/(EI_c)$ are 0.956 and 0.987, respectively. That is, the impedance damage indices are considered to have a close correlation with the equivalent bending stiffness of the cracked beam using Eq. (3).

The accuracy of the equivalent bending stiffness in Eq. (3) may be improved through future experiments on the corresponding cross section and material. Also, the cracks artificially inflicted in the above experiment are different

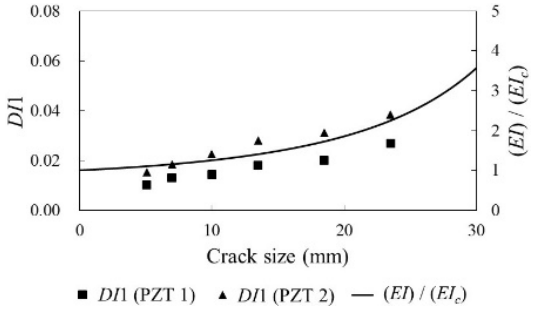

(a) $DI1$

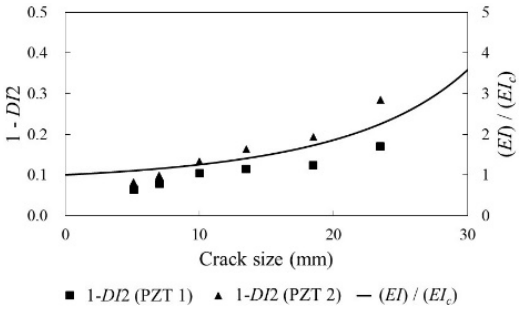

(b) $DI2$

Fig. 22 Relationship between equivalent bending stiffness and damage index

from theoretical crack. Moreover, the mechanical impedance of a structure is known to be affected by various structural properties such as damping characteristics, local mass and boundary conditions in addition to stiffness. Therefore, it is supposed that the variation in the analyzed equivalent bending stiffness according to crack progress and the variation in the impedance damage indices may not accurately agree. However, it is considered meaningful to partially identify the correlation between the impedance damage indices obtained from experiment and the analyzed equivalent bending stiffness in this study. Using this correlation, it is supposed that the structural characteristics can be more accurately evaluated from the impedance-based damage detection results, and the behavior of the structure can be effectively predicted using the analysis model.

7. Conclusions

In this study, an impedance-based damage detection method considering the temperature effect and operating conditions was experimentally researched and the correlation between the impedance damage indices obtained from experiment and the equivalent bending stiffness for the cracked beam calculated by analysis was partially identified.

The experiments were carried out in 3 stages. In the 1st stage, the experiment was carried out to estimate the effect of applied stress and vibration on the impedance signature for the healthy state. It has been found that as the degree of applied stress increases, the variation in the damage indices increases. Therefore, it is supposed that the effect of live load on impedance should be considered for the future practical application of the impedance-based damage detection method because the impedance is affected by applied stress. It has been also found that the change in the impedance signature due to vibration is insignificant and there is almost no correlation between the vibration quantity and the damage indices. In the 2nd stage, the long-term measurement under vibration was performed for the healthy state in order to evaluate the temperature effect on the impedance signature after fixing the applied stress. Damage detection with compensation of temperature effect was performed based on the results of the linear regression analysis for the data in the healthy state. The warning criterion was set considering the temperature effect and data deviation. It has been found that the damage can be clearly estimated, while monitoring the warning criterion together, after compensating the temperature effect. In the 3rd stage, the impedance was measured while increasing the crack size step by step at a crack location in order to estimate the effect of damage on the impedance signature. It has been found that as the crack size increases, the variation in the damage indices increases. Also, the correlation between the impedance damage index due to crack propagation and the analyzed equivalent bending stiffness of the cracked beam, which could be used for more accurate structural identification and prediction of structural behavior, was partially identified. These results support the usefulness of the impedance-based damage detection method for real structures.

The measurement period in this study was about 4 months, and the temperature range was not wide because it was experiment in the laboratory. In order to investigate the change of the impedance signature for a wider range of temperatures in the future, an experiment in a room with temperature control or more longer-term measurement needs to be performed. It is expected that the temperature effect on the impedance signature will be more clarified by this, and if the results of this study are applied and expanded, it will contribute to the effective practical application of the technique. In addition, further researches might address such issues as the applicability of the proposed method to various types of damages, the characteristics of impedance signature according to the distance between the crack and the PZT sensor location and the correlation between impedance signature and structural characteristics other than bending stiffness.

Acknowledgments

This work was supported by the National Research Foundation of Korea (NRF) grant funded by the Korea government (MSIT) (NRF-2022R1A2C1004708). This research was supported by Korea Electric Power Corporation. (Grant number: R20XO02-30)

References

Abbas, S., Li, F., Abbas, Z., Ur, T., Abbasi, T.U.R., Tu, X. and Pasha, R.A. (2021), "Experimental study of effect of temperature variations on the impedance signature of PZT sensors for fatigue crack detection", *Sound Vib*., **55**(1), 1-18. http://dx.doi.org/10.32604/sv.2021.013754

Antunes, R.A., Cortez, N.E., Gianesini, B.M. and Vieira Filho, J. (2019), "Modeling, simulation, experimentation, and compensation of temperature effect in impedance-based SHM systems applied to steel pipes", *Sensors*, **19**(12), 2802. http://dx.doi.org/10.3390/s19122802

Baral, S., Negi, P., Adhikari, S. and Bhalla, S. (2023), "Temperature compensation for reusable piezo configuration for condition monitoring of metallic structures: EMI approach", *Sensors*, **23**(3), 1587. http://dx.doi.org/10.3390/s23031587

Bhalla, S., Gupta, A., Bansal, S. and Garg, T. (2009), "Ultra low-cost adaptations of electro-mechanical impedance technique for structural health monitoring", *J. Intell. Mater. Syst. Struct*., **20**(8), 991-999. http://dx.doi.org/10.1177/1045389X08100384

Baptista, F.G., Filho, J.V. and Inman, D.J. (2011), "Real-time multi-sensors measurement system with temperature effects compensation for impedance-based structural health monitoring", *Struct. Health Monitor*., **11**(2), 173-186. http://dx.doi.org/10.1177/1475921711414234

Campos, F.D.S., Castro, B.A.D., Budoya, D.E., Baptista, F.G., Ulson, J.A.C. and Andreoli, A.L. (2019), "Feature extraction approach insensitive to temperature variations for impedance-based structural health monitoring", *IET Sci. Measure. Technol*., **13**(4), 536-543. http://dx.doi.org/10.1049/iet-smt.2018.5226

De Castro, B.A., Baptista, F.G. and Ciampa, F. (2019), "New signal processing approach for structural health monitoring in noisy environments based on impedance measurements", *Measurement*, **137**, 155-167. http://dx.doi.org/10.1016/j.measurement.2019.01.054

Du, F., Wu, S., Xu, C, Yang, Z. and Su, Z. (2023), "Electromechanical impedance temperature compensation and bolt loosening monitoring based on modified Unet and multitask learning", *IEEE Sensors J.*, **23**(5), 4556-4567. http://dx.doi.org/10.1109/JSEN.2021.3132943

Gianesini, B.M., Cortez, N.E., Antunes, R.A. and Vieira Filho, J. (2021), "Method for removing temperature effect in impedance-based structural health monitoring systems using polynomial regression", *Struct. Health Monitor.*, **20**(1), 202-218. http://dx.doi.org/10.1177/1475921720917126

Hong, D.S., Nguyen, K.D., Lee, I.C. and Kim, J.T. (2012), "Temperature-compensated damage monitoring by using wireless acceleration-impedance sensor nodes in steel girder connection", *Int. J. Distrib. Sensor Networks*, **8**(9), 167120. http://dx.doi.org/10.1155/2012/167120

Huynh, T.C., Dang, N.L. and Kim, J.T. (2018), "PCA-based filtering of temperature effect on impedance monitoring in prestressed tendon anchorage", *Smart Struct. Syst.*, *Int. J.*, **22**(1), 57-70. https://doi.org/10.12989/sss.2018.22.1.057

Liang, C., Sun, F. and Rogers, C.A. (1996), "Electro-mechanical impedance modeling of active material systems", *Smart Mater. Struct.*, **5**(2), 171-186. http://dx.doi.org/10.1088/0964-1726/5/2/006

Na, W.S. and Baek, J. (2018), "A review of the piezoelectric electromechanical impedance based structural health monitoring technique for engineering structures", *Sensors*, **18**(5), 1307. http://dx.doi.org/10.3390/s18051307

Rabelo, D.S., Tsuruta, K.M., De Oliveira, D.D., Cavalini, A.A., Neto, R.F. and Steffen, V. (2017), "Fault detection of a rotating shaft by using the electromechanical impedance method and a temperature compensation approach", *J. Nondestr. Eval.*, **36**, 25. http://dx.doi.org/10.1007/s10921-017-0405-9

Silva, S.D., Yano, M.O. and Gonsalez-Bueno, C.G. (2021), "Transfer component analysis for compensation of temperature effects on the impedance-based structural health monitoring", *J. Nondestr. Eval.*, **40**(3), 64. http://dx.doi.org/10.1007/s10921-021-00794-6

Tawie, P. and Lee, H.K. (2010), "Piezoelectric-based non-destructive monitoring of hydration of reinforced concrete as an indicator of bond development at the steel–concrete interface", *Cement Concrete Res.*, **40**(12), 1697-1703. http://dx.doi.org/10.1016/j.cemconres.2010.08.011

Yan, W. and Chen, W.Q. (2010), "Structural health monitoring using high-frequency electromechanical impedance signatures", *Adv. Civil Eng.*, **2010**, 429148. http://dx.doi.org/10.1155/2010/429148

Yang, X.F., Swamidas, A.S.J. and Seshadri, R. (2001), "Crack identification in vibrating beams using the energy method", *J. Sound Vib.*, **244**(2), 339-357. http://dx.doi.org/10.1006/jsvi.2000.3498

Zhang, X., Zhou, W. and Li, H. (2019), "Electromechanical impedance-based ice detection of stay cables with temperature compensation", *Struct. Control Health Monitor.*, **26**(9), e2384. http://dx.doi.org/10.1002/stc.2384